Applied Clay Science 148 (2017) 103–108

Contents lists available at ScienceDirect

Applied Clay Science

journal homepage: www.elsevier.com/locate/clay

Research paper

Preparation of functionalized kaolinite/epoxy resin nanocomposites with enhanced thermal properties

Linna Su[a], Xiaoliang Zeng[b], Hongping He[c], Qi Tao[c,d,*], Sridhar Komarneni[d]

[a] Shenzhen Polytechnic, Shenzhen 518055, PR China
[b] Shenzhen Institutes of Advanced Technology, Chinese Academy of Sciences, Shenzhen 518055, PR China
[c] CAS Key Laboratory of Mineralogy and Metallogeny & Guangdong Provincial Key Laboratory of Mineral Physics and Materials, Guangzhou Institute of Geochemistry, Chinese Academy of Sciences, Guangzhou 510640, PR China
[d] Department of Ecosystem Science and Management and Materials Research Institute, Materials Research Laboratory, The Pennsylvania State University, University Park, PA 16802, USA

ARTICLE INFO

Keywords:
Functionalized kaolinite
Epoxy resin
Nanocomposites
Thermal properties

ABSTRACT

In this study, kaolinite/epoxy resin nanocomposites were fabricated using functionalized kaolinite (KGS) as filler. The KGS was prepared by silylation of 3-aminopropyltriethoxysilane onto the surface of mechanically ground kaolinite. The addition of KGS into epoxy resin matrix improved the storage modulus and glass-transition temperature, compared to those of epoxy resin nanocomposites filled with raw kaolinite. Furthermore, with the increase of KGS loading, the coefficient of thermal expansion decreased gradually, and the dielectric constant slightly increased when compared to that of pure epoxy resin. The presence of kaolinite led to an improvement in the water resistance property of kaolinite/epoxy resin nanocomposites. This research provided guidance to construct high-performance kaolinite/epoxy resin nanocomposites.

1. Introduction

Inorganic particles-polymer nanocomposites including clay mineral-polymer nanocomposites (CPN) (Bergaya et al., 2013; Suter et al., 2015), carbon-polymer nanocomposites (Bai et al., 2011; Sun et al., 2013), ceramic-polymer nanocomposites (Dang et al., 2013), bioinspired nanocomposites (Bouville et al., 2014; Wegst et al., 2015), *etc.*, have attracted great attention during the past three decades, because they often exhibit remarkable thermal, mechanical, and barrier properties. Compared with each individual constituent, these inorganic particles-polymer nanocomposites combine the best properties of both phases, yielding potential performance well beyond those of each individual constituent material (Nair et al., 2010). Based upon these features, inorganic particles-polymer nanocomposites enjoy their applications in wide fields, such as medical devices, automotive and aerospace components, packaging, and building materials *etc.*

Among the various inorganic particles, clay minerals are one of the favorite choices, owing to their intrinsic properties such as chemical and thermal stability, easy processing, abundant resources and low cost. Since the first report on CPN in the early 1990s, there have been thousands of research investigations with the concept of clays as fillers for polymer matrices (Galimberti et al., 2013). Among them, montmorillonite is the most widely chosen filler, mainly due to its swelling property leading to exfoliation and high interlayer ion exchange capacity (Liu et al., 2011; Hasani-Sadrabadi et al., 2013; Huskic et al., 2013; Tong et al., 2014). Kaolinite is also an abundant clay mineral, which has been widely applied in ceramics, paper fillers, and also as adsorbents in pollution control processes. However, much less research has been done on kaolinite based polymer nanocomposites, compared with that on 2:1 layer type montmorillonite (Xia et al., 2010). Kaolinite is a dioctahedral 1:1 layer clay mineral with an ideal chemical formula of $Al_2Si_2O_5(OH)_4$. Its layer was constituted by superposition and bonding of a Si tetrahedral sheet with an Al octahedral sheet. Although both montmorillonite and kaolinite possess plate like structures, their cohesive energies between layers differ significantly. Kaolinite has no intercalated charge-balancing cations because of little or no isomorphous substitution in the tetrahedral and octahedral sheets unlike montmorillonite. Adjacent layers are linked by hydrogen bonds, which makes delamination or the direct intercalation of kaolinite with inorganic and/or organic molecules much harder than those of swelling clays (Tunney and Detellier, 1996; Letaief and Detellier, 2005; Detellier and Letaief, 2013). For the same reason, it is also hard to functionalize the surfaces of kaolinite leading to poor dispersion in polymer matrices. To solve these problems, a silylation reaction was performed on ground

* Corresponding author at: CAS Key Laboratory of Mineralogy and Metallogeny & Guangdong Provincial Key Laboratory of Mineral Physics and Materials, Guangzhou Institute of Geochemistry, Chinese Academy of Sciences, Guangzhou 510640, PR China.
E-mail address: taoqi@gig.ac.cn (Q. Tao).

http://dx.doi.org/10.1016/j.clay.2017.08.017
Received 2 June 2017; Received in revised form 13 August 2017; Accepted 15 August 2017

kaolinite and was successfully incorporated in polymer without re-sorting to the intercalation of highly polar, small molecules in kaolinite under severe reaction conditions (Tao et al., 2014b). The effect of such a functionalized kaolinite on epoxy curing was also evaluated by Tao et al. (2014a) who found that the addition of functionalized kaolinite could decrease activation energy and accelerate the curing reaction of epoxy resin.

In this work, kaolinite/epoxy resin (Kao/EP) nanocomposites were fabricated using KGS as filler and the effect of KGS on thermal properties of Kao/EP nanocomposites was investigated. The addition of KGS improved the thermal stability and glass-transition temperature (T_g) of the Kao/EP nanocomposites, compared to those CPN prepared by the addition of raw kaolinite. The coefficient of thermal expansion (CTE) values decreased with the increase in the KGS loading. Furthermore, the water absorption by the product decreased after the loading of KGS. This research is expected to provide guidance to construct kaolinite/polymer nanocomposite with high-performance and thus, may lead to new applications of kaolinite in polymer nanocomposites.

2. Experimental

2.1. Materials

An epoxy resin monomer, 3,4-epoxycyclohexylmethyl-3,4-epoxycyclo-hexane carboxylate (ERL 4221, Tetrachem, China) with an epoxy equivalent mass of 127.0 g mol^{-1} was used and purchased from The Dow Chemical Company. The curing agent used was methylhexahydrophthalic anhydride (MHHPA, ≥ 98%, Bangcheng CO. LTD, China) and activator was 2-ethyl-4-methylimidazole (EMI, 99%, Bangcheng CO. LTD, China). The raw kaolinite was obtained from Maoming Kaolin Science and Technology Co., LTD, China. The raw kaolinite had been already treated to remove impure minerals except quarts by supplier, and used in this study as received without further treatment. 3-Aminopropyltriethoxysilane (APTES) was purchased from Aldrich (≥ 98%) and was used as received.

2.2. Functionalization of kaolinite

A selected amount of kaolinite was ground for 6 h using a Fritsch pulverisette 5/2-type laboratory planetary mill at a rate of 370 rpm, according to a previous work (Tao et al., 2014b). 4.0 g of ground kaolinite was dispersed in 40 mL of cyclohexane and 4.0 g of APTES was slowly added into the clay dispersion under stirring. The mixture was then stirred for 24 h at 80 °C. The reaction product was collected by centrifugation and washed with cyclohexane in order to remove the excess silane. After drying at 80 °C for 24 h, the grafted product (designated as KGS) was collected for further reaction.

2.3. Preparation of the kaolinite/epoxy resin nanocomposites

KGS/epoxy resin nanocomposites with different amounts of KGS were prepared by a solvent-free method. In a typical process, a stoichiometric amount of epoxy resin, curing agent, activator, and KGS were mixed by a high speed mixer under vacuum. The uniform CPN dispersion was then gently poured into a mold, cured at 140 °C for 2 h, and then heated at 220 °C for further 2 h. The KGS loadings in the KGS/epoxy resin nanocomposites were 3 $_{wt}$%, 5 $_{wt}$% and 10 $_{wt}$%, respectively. The corresponding KGS/epoxy resin nanocomposites were designated as KGS-3/EP, KGS-5/EP, and KGS-10/EP, respectively. For comparison, pure epoxy and raw kaolinite/epoxy resin nanocomposite with 5 $_{wt}$% kaolinite loading (Kao-5/EP) were also prepared following the same procedure.

2.4. Characterization

The cross polarization magic angle spinning solid-state nuclear magnetic resonance spectra (^{29}Si CP/MAS NMR) were acquired using a Bruker Advanced 300 NMR spectrometer operating at 59.63 MHz. The contact time was 5 ms, the recycle delay was 3 s, and the spinning rate was 5.5 kHz. Tetramethylsilane was used as the external reference. The fractured surface morphologies of the CPN were examined by scanning electron microscopy (SEM, FEI Nova NanoSEM 450), working in the secondary electrons mode at a high voltage of 10 kV. The thermogravimetric analysis (TG) of the clays and CPN were conducted using a TA Instrument thermobalance (TA Q600), under 100 mL/min nitrogen flow. The samples were heated from 30 to 800 °C with a heating rate of 10 °C/min. Dynamic mechanical thermal analysis (DMA) was performed on a dynamic mechanical thermal analyzer (Q800, TA Instruments) in three-point bending mode at a frequency of 1 Hz with a constant heating rate of 3 °C/min ranging from 30 to 300 °C. Specimen dimensions were 30 mm × 6 mm × 2 mm. The T_g value was taken to be the temperature at the maximum of the tan δ peak.

The dielectric properties at room temperature were measured using an impedance analyzer (Agilent 4294A) in the frequency range of 100 Hz to 10 MHz. The samples were coated with silver paste for test. The CTE of CPN were obtained using Thermo-Mechanical Analyzer (TMA 402F3, Netzsch Instruments) by applying a force of 0.02 N with a heating rate of 10 °C/min from room temperature to 300 °C in a nitrogen atmosphere. CTE values were calculated by the following equation:

$$CTE = \frac{dL}{dT} \times \frac{1}{L_0} \quad (1)$$

where dL/dT was the slope of length-temperature curve for the sample, and L_0 is the initial length at room temperature.

Water absorption of the CPN was measured using weighing method. Firstly, the specimens with a dimension of 20 mm × 20 mm × 2 mm were put into oven at 80 °C for 24 h and then weighed. Secondly, the specimens were immersed in distilled water at a temperature of 25 °C. After 24 h, the specimens were taken out and wiped with absorbent paper to remove the water on the surfaces and then reweighed. The water absorptions (WA) of the samples were calculated by using following equation:

$$WA = \frac{W_1 - W_0}{W_0} \times 100\% \quad (2)$$

where W_0 and W_1 were the weight of dry material (the initial weight of materials prior to exposure to the water absorption) and weight of materials after exposure to water absorption, respectively.

3. Results and discussion

In a previous study, the effect of grinding on the resulting chemical structure of ground kaolinite had been investigated systematically (Tao et al., 2014b). It was demonstrated that physical grinding treatment would lead to layer disorder and fracture of kaolinite. Some interlayer surface hydroxyl groups of kaolinite would be exposed, and newly broken bonds with undercoordinated metal ions would generate after grinding, which provide new active sites for silanes to react under mild conditions. Here, solid-state ^{29}Si MAS NMR spectrum was used to identify the Si environments of the ground kaolinite and KGS (Fig. 1). Both ground kaolinite and KGS exhibit a resonance at − 92.3 ppm (Q^3[$Si(OSi)_3OM$], where M represents Al, Fe, *etc.*), corresponding to the Si in the tetrahedral clay sheets. For KGS, a new resonance was observed at − 66.7 ppm, which was attributed to the hydrolyzed tridentate bonding (T^3, [$Si(OSi)_3R$], where R = $CH_2CH_2CH_2NH_2$). This demonstrated the formation of different kinds of siloxane bonds between silane and kaolinite and among silane molecules (Tao et al., 2011). The degree of functionalization of the KGS was further estimated by TG. The thermal decomposition of KGS displayed two new mass losses at around 400 and 550 °C in the TG curves (Fig. 2). These mass losses could be attributed to the decomposition of the covalently

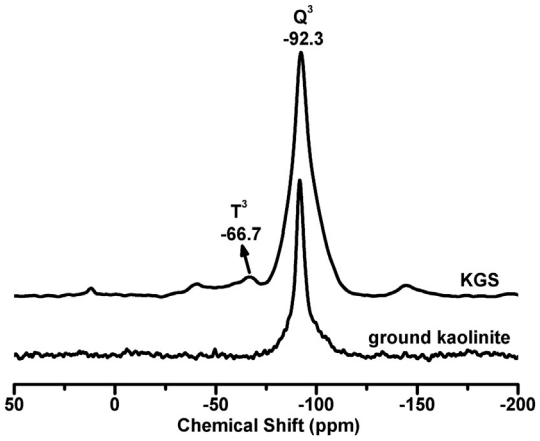

Fig. 1. ^{29}Si MAS NMR spectra of ground kaolinite and KGS.

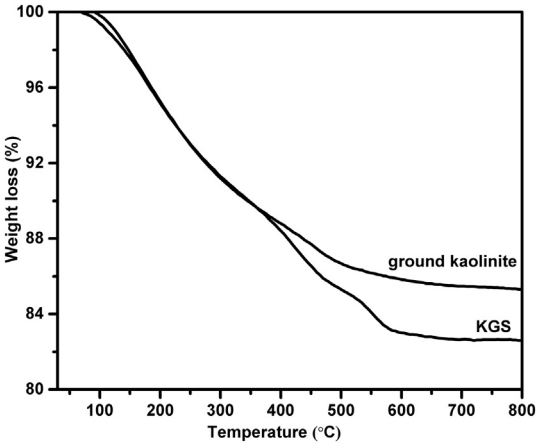

Fig. 2. TG curves of ground kaolinite and KGS.

bonded silanes on the kaolinite surface (He et al., 2005; Piscitelli et al., 2010).

SEM images showed that the fracture surface for the pure epoxy was smooth, indicating typical brittle rupture (Fig. 3a). After the addition of clay, river-like radiating patterns were displayed (Fig. 3b), suggesting an improved ductile rupture to some degree. It was interesting to note that the facture surface of the KGS/EP looked like fish scales (Fig. 3c), which was signature of ductile rupture. These fractures in the KGS/EP were possibly caused by the changing of crack direction as the cracks met with rigid KGS particles. The KGS particles played a role of bridge

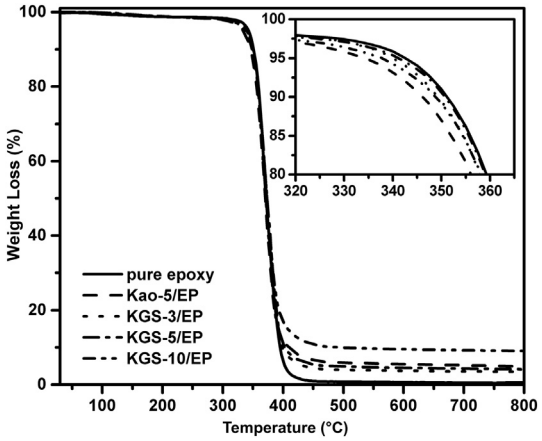

Fig. 4. TG curves of pure epoxy and clay mineral/epoxy nanocomposites.

or screw anchor in the micro cracks, preventing further extension of the crack (Liu et al., 2005; Qia et al., 2006). The appearance of these fish scales clearly indicated an improved interfacial strength between KGS and epoxy.

Thermal stability of the clay mineral/epoxy resin nanocomposites was investigated by TG measurements (Fig. 4). The pure epoxy lost 5% of its mass (onset temperature of thermal decomposition, $T_{5\%}$) at 343 °C (Table 1), which was attributed to the degradation of methyl methylene groups in the epoxy resin molecules. With the increased temperature, TG curve of the pure epoxy showed a sharp drop in trend, corresponding to the degradation of alkyl chain. When the temperature was over 400 °C, the mass loss rate of each system was significantly decreased, indicating that most of the groups in epoxy resin structure have been thermally decomposed. After the addition of clay, either raw kaolinite or KGS, the $T_{5\%}$ values reduced to 335 °C and 340 °C for Kao-5/EP and KGS-5/EP, respectively. This was possibly due to the decreased cross-linking density of epoxy resins caused by the addition of clay (Gua and Liang, 2003; Becker et al., 2004; Brnardić et al., 2008). On the other hand, the KGS/EP showed higher thermal stability than Kao/EP, which indicated that the grafted silane enhanced the compatibility of kaolinite with epoxy resin. Furthermore, the char yields of the clay mineral/epoxy resin nanocomposites at about 500 °C were all higher than that of pure epoxy, because of the clay residues.

DMA is an effective approach to evaluate the physical and chemical properties of inorganic particles-polymer nanocomposites. Understanding temperature curve of the G' (storage modulus), G'' (loss modulus), and tan δ (G''/G') can provide valuable insights into the toughness of a material as well as the molecular relaxation (Gonzalez-Dominguez et al., 2011). The DMA curves of the clay mineral/epoxy

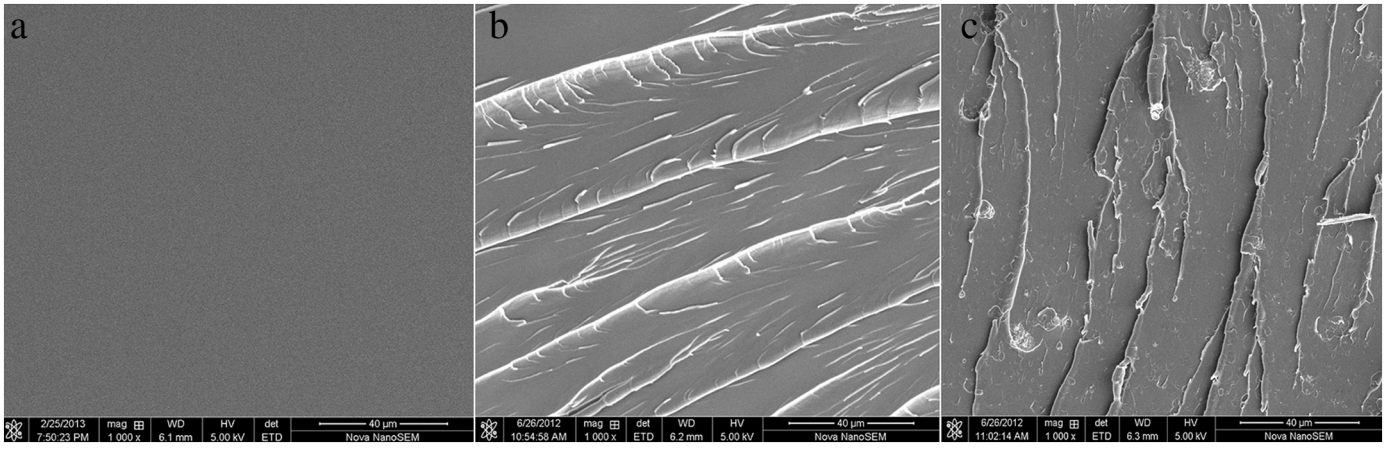

Fig. 3. SEM images of fracture surfaces of pure epoxy: (a), Kao-5/EP (b), and KGS-5/EP (c).

Table 1
Temperature at 5 $_{wt}$% weight loss, storage modulus and T_g results of pure epoxy and clay mineral/epoxy nanocomposites.

Samples	$T_{5\%}$ (°C)	Storages(30 °C, MPa)	T_g (°C)
pure epoxy	343	1674	223
KGS-3/EP	340	1805	231
KGS-5/EP	341	2019	226
KGS-10/EP	338	2085	227
Kao-5/EP	335	1754	225

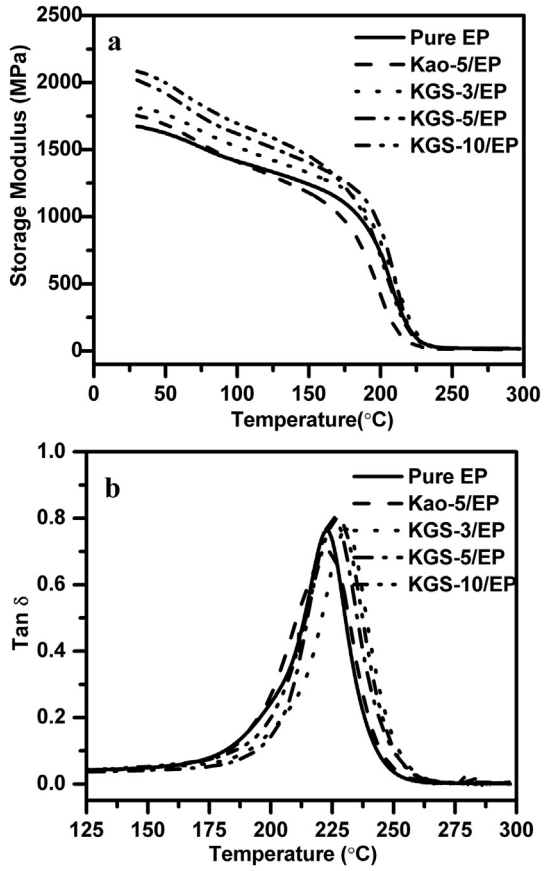

Fig. 5. Storage modulus (a) and tan δ (b) *versus* temperature of pure epoxy and clay mineral/epoxy nanocomposites.

resin nanocomposites were presented in Fig. 5. The relative changes in G' of the clay mineral/epoxy resin nanocomposites at 30 °C were summarized in Table 1. The incorporation of KGS resulted in an increase of G', *e.g.*, from 1674 MPa for pure epoxy to 2085 MPa at 10 $_{wt}$% KGS in the glassy state at 30 °C. The increased of G' was attributed to the reinforcement effect of the KGS on the epoxy resin, since the KGS can restrict the mobility of the epoxy polymer chains and provide additional stress transfer under loading (An et al., 2008; Sebenik et al., 2015). In addition, KGS/EP nanocomposites had higher G' values than that of Kao/EP nanocomposites. The enhanced interfacial interaction between KGS and epoxy could immobilize more epoxy resin chains and provide more load transfer centers. The G' decreased at higher temperatures, manifesting a rubbery state of the KGS/EP nanocomposites. As can be seen in Fig. 5b, the KGS/EP nanocomposites displayed one transition peak in the loss modulus and the tan δ curves, indicating that phase separation does not occur between epoxy and KGS.

Glass transition temperature (T_g), which is one of the most important properties of epoxy resins, provides information on the fundamental changes in the polymer chain dynamics and thermal stability of the material. The T_g value could be defined as the temperature

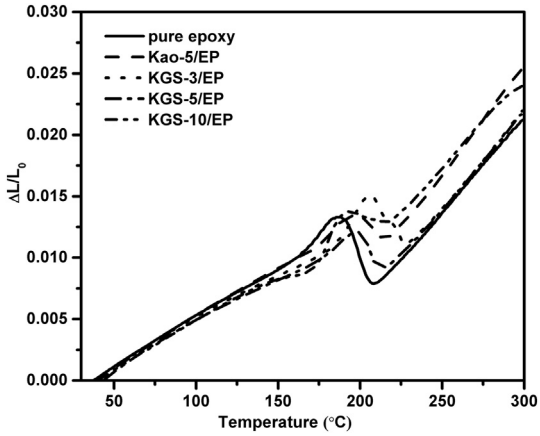

Fig. 6. TMA curves of the pure epoxy and clay mineral/epoxy nanocomposites.

corresponding to the peak maximum of the loss modulus or of the tan δ. As shown in Table, the addition of KGS led to a higher T_g compared with the pure epoxy. The maximum value of T_g located at 231 °C with 3 $_{wt}$% KGS was about 8 °C higher than the T_g of pure epoxy (223 °C). The slight increase of T_g value of clay mineral/epoxy resin nanocomposites might be due to the interaction of clay with the epoxy network which could restrict the chain mobility. Afterwards, T_g slightly decreased as the filler loading increased, which was probably related to some aggregation of KGS. In addition, at the some filler loading (5 $_{wt}$%), the CPN filled with KGS showed higher T_g (226 °C) than that of the CPN filled with raw kaolinite (225 °C). The presence of silane in KGS might promote the polymerization of KGS/EP nanocomposites, which may have led to a better KGS dispersion in epoxy network (Tao et al., 2014a). This further indicated an enhanced interfacial interaction between KGS and epoxy.

CTE was an important issue for polymers in engineering applications (Jang et al., 2012). A low CTE was helpful for materials to keep dimensional stability. The effect of KGS on the thermal dimensional stability of epoxy resins was examined by TMA (Fig. 6). The slopes of the length-temperature curves for all of the samples exhibit a gradual change as a function of temperature, which represented the transition from the glassy state to the rubbery state. The CTE values of the Kao/EP nanocomposites were calculated from the slope of the thermal expansion curves below and above T_g in the temperature regions of 40–150 °C and 250–300 °C, respectively (Table 2). The CTE values of the KGS/epoxy resin nanocomposites decreased monotonically with increased KGS loading. The largest CTE reduction occurred at the highest filler loading as expected, which decreased from 80.0 ppm/°C below T_g and 201 ppm/°C above T_g for pure epoxy to 60.0 ppm/°C and 154 ppm/°C at 10 $_{wt}$% KGS. Such a decrease in the CTE was attributed to the intrinsic lower CTE of the rigid kaolinite and the polymer chains bounded and constrained by the fillers. In addition, it was observed that at the same filler loading (5 $_{wt}$%), the CPN filled with KGS had lower CTE than that of the raw kaolinite/epoxy resin nanocomposites, suggesting that the functionalization was beneficial to improve the interfacial strength between kaolinite and epoxy.

Dielectric properties including dielectric constant and dielectric loss

Table 2
CTE values of pure epoxy and clay mineral/epoxy nanocomposites.

Samples	CTE 1(10^{-6}/°C)	CTE 2(10^{-6}/°C)
Pure epoxy	80.0	201.0
KGS-3/EP	78.0	187.0
KGS-5/EP	69.5	172.0
KGS-10/EP	60.0	154.0
Kao-5/EP	80.4	191.0

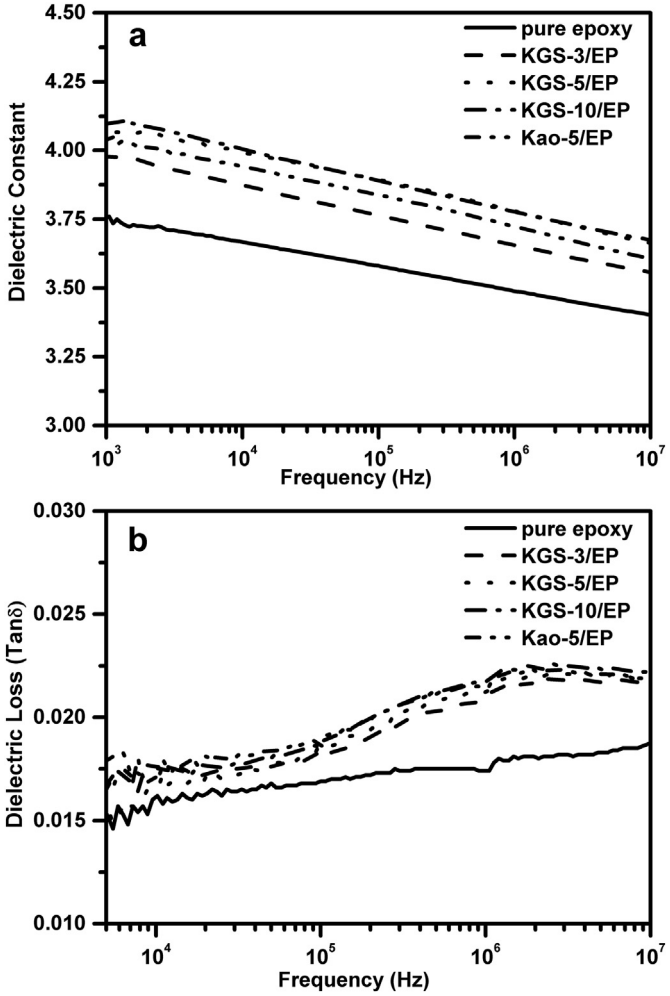

Fig. 7. Dielectric constant *versus* frequency (a) and dielectric loss *versus* frequency (b) of the pure epoxy and clay mineral/epoxy nanocomposites.

are one of the most important properties for CPN. The dielectric constant represents the ability of storing electric charges in the electric field, while the dielectric loss reflects the consumption of energy resulting from the electrical current generated in the conductive carriers under the alternating electric field (Cao et al., 2015). For CPN with different kaolinite loadings, the dielectric constant decreased with increasing frequency (Fig. 7), which was ascribed to an interfacial relaxation (Chen et al., 2015). The addition of KGS led to increase in dielectric constant, *i.e.*, from ~ 3.5 for the pure epoxy resins to ~ 3.8 for the KGS-10/EP (Fig. 7a). This was because of the higher dielectric constant of kaolinite than that of pure epoxy resin. At the same kaolinite loading (5.0 $_{wt}$%), KGS-5/EP had a lower dielectric constant than that of Kao-5/EP. The difference in the dielectric properties between KGS-5/EP and Kao-5/EP was believed to result from a difference in interfacial interaction. The surface modification of kaolinite led to stronger interfacial interaction between KGS and epoxy resins compared with that of Kao-5/EP. Generally, strong interfacial interaction was beneficial to limit the polarization movement of dipoles, and thus leading to low dielectric constant. The dielectric loss of all the studied CPN increased with increasing frequency (Fig. 7b). This was because the rotational motions of dipolar groups could not catch up with the frequency change of the electric field (Xu et al., 2010). After the addition of KGS, the dielectric loss of the KGS/epoxy resin nanocomposites slightly increased with KGS loadings. Moreover, the surface modification was beneficial to reducing the dielectric loss. Although the dielectric loss increased with further increases in frequency, it was still < 0.05, showing that the material could have a potential application in electronic information industry.

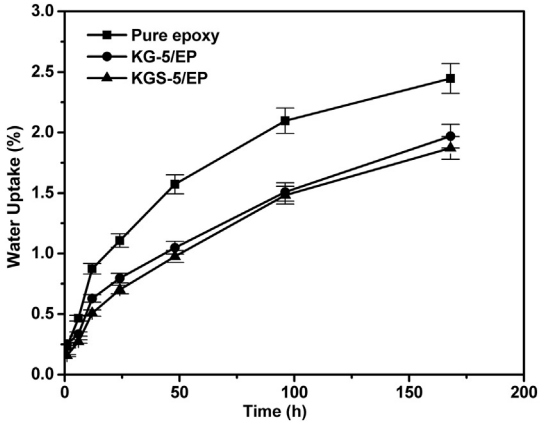

Fig. 8. Water uptake curves of pure epoxy and clay mineral/epoxy nanocomposites.

Absorbed water trapped in CPN would deteriorate their long term performance, therefore it is very crucial to reduce the water uptake of the CPN and avoid such a problem. The effect of clay on the water absorption for clay mineral/epoxy resin nanocomposites was studied as a function of the immersion time (Fig. 8). The water absorption of pure epoxy was relatively higher compared to clay mineral/epoxy resin nanocomposites. For the pure epoxy resin, the water absorption increased by prolonging the immersion time, and reached 2.4 $_{wt}$% after immersion for 168 h. For clay mineral/epoxy nanocomposites, although water absorptions also increased with extension of immersion time, they were lower than those for pure epoxy. Water absorption might be due to the capability of the water molecules to penetrate through the epoxy network (Becker et al., 2004). If the epoxy resin did not contain clay, the water molecules tended to go into the voids or defects of the epoxy matrix from the surface when exposed to saturated moisture, and then spread inside the matrix of pure epoxy (Jia et al., 2015). The presence of clay promoted the polymerization, which resulted in increasing of the tortuosity path for water penetration since water molecules could not penetrate the clay platelets and thus improved water resistance properties (Tao et al., 2014a; Jia et al., 2015). In addition, the water absorptions of KGS/EP were slightly lower than those of Kao/EP, indicating that the KGS was beneficial to water separation. A possible interpretation was that the introduction of the silane groups on the surface of kaolinite might restrict access to some sites and also effectively reduce the microvoid volume available for water.

4. Conclusions

Functionalized kaolinite/epoxy resin nanocomposites were fabricated using functionalized kaolinite as filler. The KGS/EP nanocomposite had higher G' values than that of raw kaolinite filled epoxy nanocomposite. The enhanced interfacial interaction between KGS and epoxy could immobilize more epoxy resin chains and provide more load transfer centers. At the same amount of filler loading (5 $_{wt}$%), the CPN filled with KGS showed higher T_g than that of the kaolinite/epoxy resin nanocomposites filled with raw kaolinite, indicating an enhanced interfacial interaction between KGS and epoxy. The TG measurements showed that the addition of clay led to the slight reduction of the $T_{5\%}$ of kaolinite/epoxy resin nanocomposites, due to the decreased cross-linking density of epoxy resins. At the same filler loading (5 $_{wt}$%), the KGS/EP nanocomposites had lower CTE than that of raw kaolinite/epoxy resin nanocomposites. The KGS/EP nanocomposites had lower dielectric constant than that of the Kao/EP nanocomposites as a result of reduction of the surface polarization by surface functionalization. The KGS was beneficial to water separation and led to lower water absorption by KGS/EP nanocomposite than that of Kao/EP

nanocomposites. These results demonstrated that the surface functionalization of kaolinite is a simple but effective approach to obtain high performance clay mineral-polymer nanocomposites.

Acknowledgments

This work was financially supported by the Foundation of Shenzhen Polytechnic (no. 6017-22 K210169991) and National Natural Science Foundation of China (Grant nos. 41572031, 41322014, and 21177104).

References

An, L., Pan, Y.Z., Shen, X.W., Lu, H.B., Yang, Y.L., 2008. Rod-like attapulgite/polyimide nanocomposites with simultaneously improved strength, toughness, thermal stability and related mechanisms. J. Mater. Chem. 18, 4928–4941.

Bai, H., Li, C., Shi, G., 2011. Functional composite materials based on chemically converted graphene. Adv. Mater. 23, 1089–1115.

Becker, O., Varley, R.J., Simon, G.P., 2004. Thermal stability and water uptake of high performance epoxy layered silicate nanocomposites. Eur. Polym. J. 40, 187–195.

Bergaya, F., Detellier, C., Lambert, J.F., Lagaly, G., 2013. Introduction to clay-polymer nanocomposites (CPN) (Chapter 13.0). In: Bergaya, F., Lagaly, G. (Eds.), Handbook of Clay Science. Developments in Clay Science. vol. 5A Elsevier.

Bouville, F., Maire, E., Meille, S., Van de Moortele, B., Stevenson, A.J., Deville, S., 2014. Strong, tough and stiff bioinspired ceramics from brittle constituents. Nat. Mater. 13, 508–514.

Brnardić, I., Macan, J., Ivanković, H., Ivanković, M., 2008. Thermal degradation kinetics of epoxy/organically modified montmorillonite nanocomposites. J. Appl. Polym. Sci. 107, 1932–1938.

Cao, T., Yuan, L., Gu, A., Liang, G., 2015. Fabrication and origin of new flame retarding bismaleimide resin system with low dielectric constant and loss based on microencapsulated hexaphenoxycyclotriphosphazene in low phosphorus content. Polym. Degrad. Stab. 121, 157–170.

Chen, X., Yuan, L., Zhang, Z., Wang, H., Liang, G., Gu, A., 2015. New glass fiber/bismaleimide composites with significantly improved flame retardancy, higher mechanical strength and lower dielectric loss. Compos. B Eng. 71, 96–102.

Dang, Z.-M., Yuan, J.-K., Yao, S.-H., Liao, R.-J., 2013. Flexible nanodielectric materials with high permittivity for power energy storage. Adv. Mater. 25, 6334–6365.

Detellier, C., Letaief, S., 2013. Kaolinite-polymer nanocomposites (Chapter 13.2). In: Bergaya, F., Lagaly, G. (Eds.), Handbook of Clay Science. Developments in Clay Science. vol. 5A Elsevier.

Galimberti, M., Cipolletti, V.R., Coombs, M., 2013. Applications of clay-polymer nanocomposites (Chapter 4.4). In: Bergaya, F., Lagaly, G. (Eds.), Handbook of Clay Science. Developments in Clay Science. vol. 5B Elsevier.

Gonzalez-Dominguez, J.M., Anson-Casaos, A., Diez-Pascual, A.M., Ashrafi, B., Naffakh, M., Backman, D., Stadler, H., Johnston, A., Gomez, M., Martinez, M.T., 2011. Solvent-free preparation of high-toughness epoxy-SWNT composite materials. ACS Appl. Mater. Interfaces 3, 1441–1450.

Gua, A., Liang, G., 2003. Thermal degradation behaviour and kinetic analysis of epoxy/montmorillonite nanocomposites. Polym. Degrad. Stab. 80, 383–391.

Hasani-Sadrabadi, M.M., Ghaffarian, S.R., Renaud, P., 2013. Nafion/benzotriazole functionalized montmorillonite nanocomposites: novel high-performance proton exchange membranes. RSC Adv. 3, 19357–19365.

He, H., Duchet, J., Galy, J., Gerard, J.-F., 2005. Grafting of swelling clay materials with 3-aminopropyltriethoxysilane. J. Colloid Interface Sci. 288, 171–176.

Huskic, M., Zigon, M., Ivankovic, M., 2013. Comparison of the properties of clay polymer nanocomposites prepared by montmorillonite modified by silane and by quaternary ammonium salts. Appl. Clay Sci. 85, 109–115.

Jang, J.-S., Bouveret, B., Suhr, J., Gibson, R.F., 2012. Combined numerical/experimental investigation of particle diameter and interphase effects on coefficient of thermal expansion and young's modulus of SiO_2/epoxy nanocomposites. Polym. Compos. 33, 1415–1423.

Jia, X., Zheng, J., Lin, S., Li, W., Cai, Q., Sui, G., Yang, X., 2015. Highly moisture-resistant epoxy composites: an approach based on liquid nano-reinforcement containing well-dispersed activated montmorillonite. RSC Adv. 5, 44853–44864.

Letaief, S., Detellier, C., 2005. Reactivity of kaolinite in ionic liquids: preparation and characterization of a 1-ethyl pyridinium chloride-kaolinite intercalate. J. Mater. Chem. 15, 4734–4740.

Liu, W., Hoa, S.V., Pugh, M., 2005. Organoclay-modified high performance epoxy nanocomposites. Compos. Sci. Technol. 65, 307–316.

Liu, M., Zhang, X., Zammarano, M., Gilman, J.W., Davis, R.D., Kashiwagi, T., 2011. Effect of montmorillonite dispersion on flammability properties of poly(styrene-co-acrylonitrile) nanocomposites. Polymer 52, 3092–3103.

Nair, B.P., Pavithran, C., Sudha, J.D., Prasad, V.S., 2010. Microvesides through self-assembly of polystyrene-clay nanocomposite. Langmuir 26, 1431–1434.

Piscitelli, F., Posocco, P., Toth, R., Fermeglia, M., Pricl, S., Mensitieri, G., Lavorgn, M., 2010. Sodium montmorillonite silylation: unexpected effect of the aminosilane chain length. J. Colloid Interface Sci. 351, 108–115.

Qia, B., Zhang, Q.X., Bannister, M., Mai, Y.-W., 2006. Investigation of the mechanical properties of DGEBA-based epoxy resin with nanoclay additives. Compos. Struct. 75, 514–519.

Sebenik, G., Huskic, M., Vengust, D., Zigon, M., 2015. Properties of epoxy and unsaturated polyester nanocomposites with polycation modified montmorillonites. Appl. Clay Sci. 109, 143–150.

Sun, X., Sun, H., Li, H., Peng, H., 2013. Developing polymer composite materials: carbon nanotubes or graphene? Adv. Mater. 25, 5153–5176.

Suter, J.L., Groen, D., Coveney, P.V., 2015. Chemically specific multiscale modeling of clay-polymer nanocomposites reveals intercalation dynamics, tactoid self-assembly and emergent materials properties. Adv. Mater. 27, 966–984.

Tao, Q., Zhu, J.X., Wellard, R.M., Bostrom, T.E., Frost, R.L., Yuana, P., He, H.P., 2011. Silylation of layered double hydroxidesvia an induced hydrolysis method. J. Mater. Chem. 21, 10711–10719.

Tao, Q., Su, L., Frost, R.L., He, H., Theng, B.K.G., 2014a. Effect of functionalized kaolinite on the curing kinetics of cycloaliphatic epoxy/anhydride system. Appl. Clay Sci. 95, 317–322.

Tao, Q., Su, L.N., Frost, R.L., Zhang, D., Chen, M.Y., Shen, W., He, H.P., 2014b. Silylation of mechanically ground kaolinite. Clay Miner. 49, 559–568.

Tong, Z.-Z., Zhou, B., Huang, J., Xu, J.-T., Fan, Z.-Q., 2014. Hierarchical structures of olefinic blocky copolymer/montmorillonite nanocomposites with collapsed and intercalated clay layers. RSC Adv. 4, 15678–15688.

Tunney, J.J., Detellier, C., 1996. Chemically modified kaolinite. Grafting of methoxy groups on the interlamellar aluminol surface of kaolinite. J. Mater. Chem. 6, 1679–1685.

Wegst, U.G.K., Bai, H., Saiz, E., Tomsia, A.P., Ritchie, R.O., 2015. Bioinspired structural materials. Nat. Mater. 14, 23–36.

Xia, X., Zeng, X., Liu, J., Xu, W., 2010. Preparation and characterization of epoxy/kaolinite nanocomposites. J. Appl. Polym. Sci. 118, 2461–2466.

Xu, H.-P., Dang, Z.-M., Bing, N.-C., Wu, Y.-H., Yang, D.-D., 2010. Temperature dependence of electric and dielectric behaviors of Ni/polyvinylidene fluoride composites. J. Appl. Phys. 107, 034105.